

Tuning exchange bias in Fe/ γ -Fe₂O₃ core-shell nanoparticles: Impacts of interface and surface spins

Hafsa Khurshid,^{a)} Manh-Huong Phan,^{a)} Pritish Mukherjee, and Hariharan Srikanth^{a)}
 Department of Physics, University of South Florida, Tampa, Florida 33620, USA

(Received 3 January 2014; accepted 3 February 2014; published online 19 February 2014)

A comparative study has been performed of the exchange bias (EB) effect in Fe/ γ -Fe₂O₃ core-shell nanoparticles with the same thickness of the γ -Fe₂O₃ shell (~ 2 nm) and the diameter of the Fe core varying from 4 nm to 11 nm. Transmission electron microscopy (TEM) and high-resolution TEM confirmed the high quality of the core-shell nanostructures. A systematic analysis of magnetization versus magnetic field measurements under zero-field-cooled and field-cooled regimes using the Meiklejohn-Bean model and deconvoluting superparamagnetic and paramagnetic contribution to the total magnetic moment Langevin function shows that there exists a critical particle size (~ 10 nm), above which the spins at the interface between Fe and γ -Fe₂O₃ contribute primarily to the EB, but below which the surface spin effect is dominant. Our finding yields deeper insight into the collective contributions of interface and surface spins to the EB in core-shell nanoparticle systems, knowledge of which is the key to manipulating EB in magnetic nanostructures for spintronics applications. © 2014 AIP Publishing LLC. [<http://dx.doi.org/10.1063/1.4865904>]

Exchange bias (EB) in magnetic nanostructures is of current interest because of its potential use in spin valves, magnetoresistive random-access memory (MRAM) circuits, magnetic tunnel junctions, and spintronic devices.^{1–3} It is also an unavoidable consequence of nanostructuring, in many cases, due to the large relative fraction of surface and interface spins compared to the total volume.² Despite its technological impact, the physical origin of EB is not fully understood.^{2,4–6} An example of this is the case of γ -Fe₂O₃ nanoparticles^{7,8} and their composites,^{9–15} where the degree of disorder of the surface spins in the outer layer to which the ferromagnetically ordered spins of the core are coupled is believed to be crucial for achieving EB.² Martinez *et al.* reported that due to their very high surface to volume ratio, γ -Fe₂O₃ nanoparticles possessed highly disordered surface spins that underwent a low temperature spin-glass-like transition (T_F) below which both strong exchange anisotropy and EB effect were observed.⁷ A similar trend was reported later by Shendruk *et al.*, who otherwise proved the surface spin disorder as a major cause for the unusual exponent-like decrease of the γ -Fe₂O₃ nanoparticle's saturation magnetization (M_S) with increasing temperature.⁸ A more complicated situation is found when γ -Fe₂O₃ nanoparticles are coated with non-magnetic and magnetic layers.^{9–15} In one case, coating the surface of γ -Fe₂O₃ nanoparticles with a non-magnetic layer such as Cu was reported to significantly reduce surface spin disorder (or enhance surface spin stability), the result of which was the remarkable decrease of the EB field observed for Cu-coated γ -Fe₂O₃ nanoparticles.^{9,10} In another case, frozen spins at the interface between γ -Fe₂O₃ nanoparticles and other magnetic components such as Fe, CoO, and Fe₃O₄, in the corresponding core-shell Fe/ γ -Fe₂O₃,^{11,12} CoO/ γ -Fe₂O₃,¹³ and Fe₃O₄/ γ -Fe₂O₃¹⁴ nanostructures, are also believed to contribute to the observed EB effects.^{15–17} These diverse observations raise a very

important and fundamental question of how to decouple collective contributions of the interface and surface spins to the EB in these core-shell nanoparticle systems, knowledge of which is essential to tailor EB in magnetic nanostructures for spintronics applications. To address this emerging issue, it is necessary to perform a comparative study of the EB in a core-shell nanoparticle system by keeping the same thickness of the shell, while varying the diameter of the core.

In this Letter, through a comprehensive study of the EB in ferromagnetic/ferrimagnetic (FM/FIM) Fe/ γ -Fe₂O₃ core/shell nanoparticles with varying particle sizes (8 nm–15 nm), we demonstrate that there exists a critical particle size (~ 10 nm), above which the interface spin effect dominates the EB, but below which the surface spin effect becomes more important. This finding sheds light on the origin of the observed EB effects and provides a path towards tuning EB in core/shell nanostructures for spintronics applications.

Fe/ γ -Fe₂O₃ core/shell nanoparticles were synthesized by following the well-established standard synthesis technique of thermal decomposition of iron pentacarbonyl¹⁸ at high temperature. Details of the synthesis method have been reported elsewhere.¹⁹ The average particle size was varied by changing the oleylamine concentration. The iron precursor injection temperature and the refluxing temperature were kept at 220 °C for all the samples. Figure 1 shows the transmission electron microscopy (TEM) images along with high-resolution TEM (HRTEM) images of (a) 14.8 ± 1.1 nm, (c) 9.9 ± 1.2 nm, and (d) 7.7 ± 1.6 nm nanoparticles (denoted as samples A-15, A-10, and A-8, respectively). In agreement with our earlier study,¹² the core is made up of metallic Fe⁽⁰⁾ and the shell is composed of randomly oriented grains of γ -Fe₂O₃. With the variation of average particle size from ~ 15 nm to ~ 8 nm, the average diameter of the Fe core varies from ~ 11 nm to ~ 4 nm, while the thickness of the γ -Fe₂O₃ shell remains the same (~ 2 nm).

Figure 2 shows the temperature dependence of magnetization (M-T), measured under the zero-field-cooled (ZFC) and field-cooled (FC) protocols in a field of 100 Oe, for all

^{a)}Authors to whom correspondence should be addressed. Electronic addresses: hkhurshi@usf.edu; phanm@usf.edu; and sharihar@usf.edu

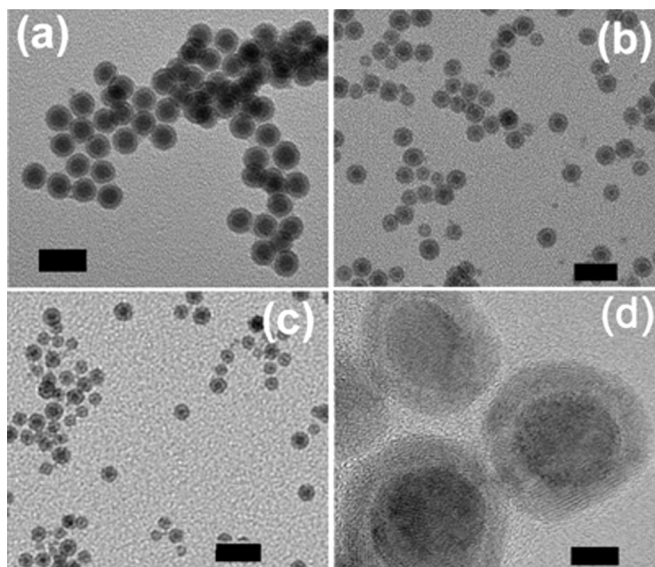


FIG. 1. TEM images of Fe/ γ -Fe₂O₃ nanoparticle samples with an average size of (a) 15 nm, (b) 10 nm, and (c) 8 nm. An HRTEM image is shown for the 10 nm particles. The scale bar is 20 nm for (a)-(c).

samples investigated. It can be seen that the ZFC M-T curves show a maximum at a certain temperature (T_{P-ZFC}), which shifts towards lower temperature with the decrease in particle size; 110 K for 15 nm (a), 67 K for 10 nm (b), and 48 K for 8 nm (c). Under the ideal condition of non-interacting, monodisperse particles, the peak in a ZFC M-T curve is often referred as to the mean blocking temperature (T_B). This is associated with the maximum number of nanoparticles unblocking as temperature increases and is found to occur when the thermal energy ($k_B T$) is comparable to the activation energy (E_a). However, for core-shell nanoparticles with strong inter- and intra-particle interactions and finite size

distribution, T_{P-ZFC} may be broadened and shifts to higher values due to enhanced interactions.² As a result, the peak (T_{P-ZFC}) may not accurately represent T_B of the system,¹² which can thus be estimated from $\frac{d(M_{FCW}-M_{ZFC})}{dT}$ (Fig. 2(c)), and yields 75 K, 58 K, and 36 K for samples A-15, A-10, and A-8, respectively. Since T_B is proportional to the anisotropy constant (K_u) and magnetic volume (V) of the particle via $T_B = K_u V / 25 k_B$, where k_B is the Boltzmann constant, the decrease of T_B with the decrease in particle size in the present case is attributed to the decrease in the magnetic volume of the particle.⁵ The close coincidence of the ZFC peak and the onset of the irreversibility between the ZFC and FC M-T curves are observed for all the samples, which is indicative of the absence of particle aggregation or large variation in size distribution,^{2,12} and is fully consistent with the TEM characterization (Fig. 1).

For samples A-15 and A-10, the FC M-T curves show, in addition to a maximum around T_1 , a sharp increase in the FC magnetization below T_2 (see Figs. 2(a) and 2(b) and their insets). A similar feature has also been reported previously in γ -Fe₂O₃ and Fe/ γ -Fe₂O₃ core/shell nanoparticles, which has been attributed to the onset of the freezing process of disordered surface spins (S_f).^{7,11,12} For the smallest particles (sample A-8), the continuous increase of the FC magnetization with lowering temperature is likely a result of the dominant effect of disordered surface spins. These features can be reconciled with those seen in the magnetization versus magnetic field (M-H) curves taken at 5 K (see Fig. 2(d)). We find that the decreasing particle size significantly decreases the magnetization and increases the magnetic anisotropy. The 5 T magnetization at 5 K decreases from 30 emu/g for the 15 nm particles to 5 emu/g for the 8 nm particles. The non-saturation behavior of the magnetization appears in all samples, with the strongest effect observed in the smallest

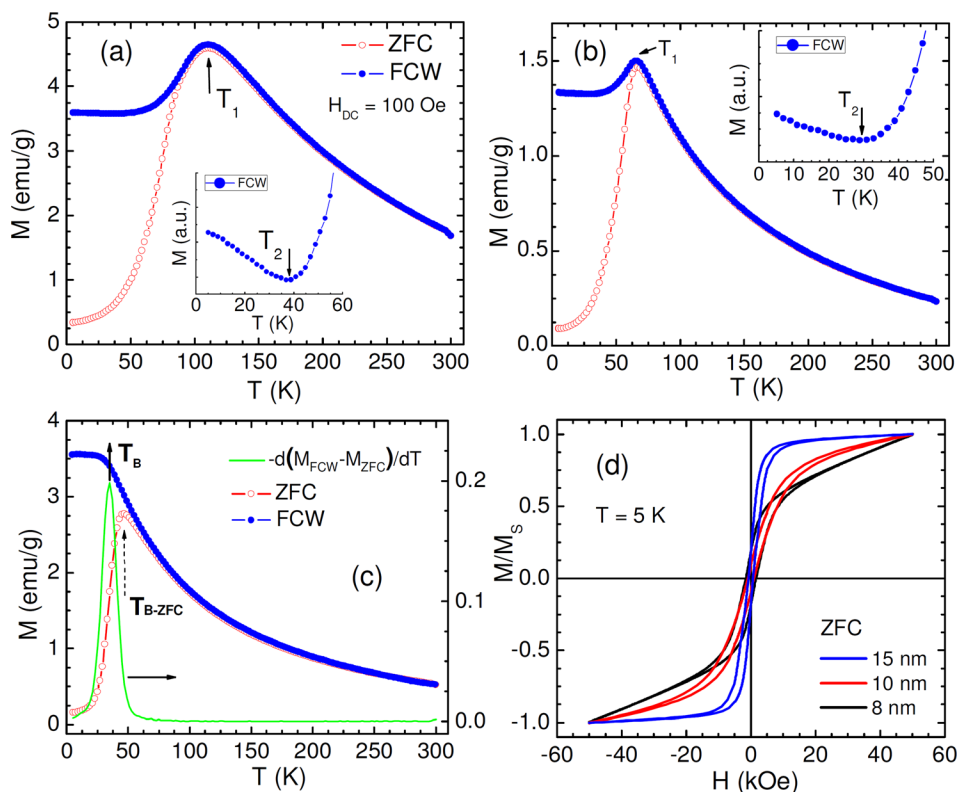


FIG. 2. Temperature dependence of ZFC and FC magnetization taken at a field of 100 Oe for (a) 15 nm, (b) 10 nm, and (c) 8 nm Fe/ γ -Fe₂O₃ nanoparticles. Insets (a) and (b) show the enlarged portion of the FC M-T curves. The derivative of magnetization with respect to temperature (dM/dT) is also shown in Fig. 2(c). The magnetic loops taken at 5 K are shown in Fig. 2(d).

particles (see Fig. 2(d)). These results suggest an enhanced disordering effect of surface spins in samples with reduced particle size.²

Nanoparticle systems that show features of surface spin disorder often have an exchange anisotropy induced by a disordered spin phase that is manifest as an EB after cooling in a field.^{2,7,8,11,12} To investigate EB in these nanoparticles, the samples were cooled from room temperature in the presence of a magnetic field. Figure 3(a) and its inset show, for example, the FC and ZFC M-H loops taken at 5 K (main panel) and the FC M-H loops at different temperatures below T_B (inset) for sample A-10. A clear shift of the FC M-H loop along the negative field axis indicates the presence of a strong EB effect in the nanoparticle system. The EB field is calculated as $H_{EB} = \left[\frac{|H^+ + H^-|}{2} \right]$, where H^+ and H^- are the coercive fields for the ascending and descending curves, respectively. Figures 3(b)–3(d) show the temperature dependence of EB field measured in a cooling field of 5 T for all the samples. It can be seen that H_{EB} decreases exponentially with temperature for all the samples. A similar trend has also been reported on other exchange-biased particle systems.^{15,16} It is very interesting to note in Figs. 3(b)–3(d) that with the decrease in particle size from 15 nm to 8 nm, H_{EB} first increases significantly, reaches a maximum for 10 nm, and then decreases for smaller particles. The values of H_{EB} are calculated at 5 K to be 1.6 kOe, 3.5 kOe, and 3.2 kOe for 15 nm, 10 nm, and for 8 nm. The total EB effect should be attributed to the combined contributions from interface and surface spin effects as noted above.

In order to quantify contribution to the EB from the interface spin effect for the case of our nanoparticle systems, we have used the modified Meiklejohn and Bean (MB) model, which was initially developed for EB in antiferromagnetic (AFM)/FM coupled thin films,²⁰ and has recently

been extended to the case of core/shell nanoparticles.²¹ It has been pointed out that a small but significant number of aligned frozen spins between the core and the shell layers can have a strong impact on EB in core/shell particle systems.^{15,21–23} In the case of our Fe/ γ -Fe₂O₃ nanoparticles, the decrease in particle size is expected to vary the interaction area between the Fe core and the γ -Fe₂O₃ shell within the nanoparticles, thus leading to a variation in the relative population of interfacial frozen spins. According to the modified MB model,²¹ the H_{EB} in a core/shell (FM/FIM) nanoparticle system can be written as

$$H_{EB} = 2 \frac{nJ_{ex}S_{FM}S_{FIM}}{a^2M_{FM}t_{FM}} = \frac{\Delta E}{2M_{FM}t_{FM}}, \quad (1)$$

where ΔE is the interfacial exchange-energy density needed to reverse the frozen spins and J_{ex} is the interfacial exchange constant. S_{FM} and S_{FIM} represent individual spin moments of the FM core and the FIM shell, respectively. M_{FM} and t_{FM} are the saturation magnetization and effective thickness of the ferromagnetic layer, and n/a^2 is the number of exchange-coupled bonds across the interface per unit area. In the case of our Fe/ γ -Fe₂O₃ nanoparticles, the interfacial spins between two different magnetically ordered layers (Fe and γ -Fe₂O₃) play the critical role of irreversible spins frozen with a magnetic field, while the moment of the Fe core spins is reversible with the field. The number of exchange-coupled spins increases with the number of frozen spins and hence interfacial exchange-energy density. In addition to the horizontal shift, a vertical shift in the FC M-H loop is representative of the frozen spins that cannot be reversed by the measurement field. Therefore, the net moment of these frozen spins (M_f) can be quantified as

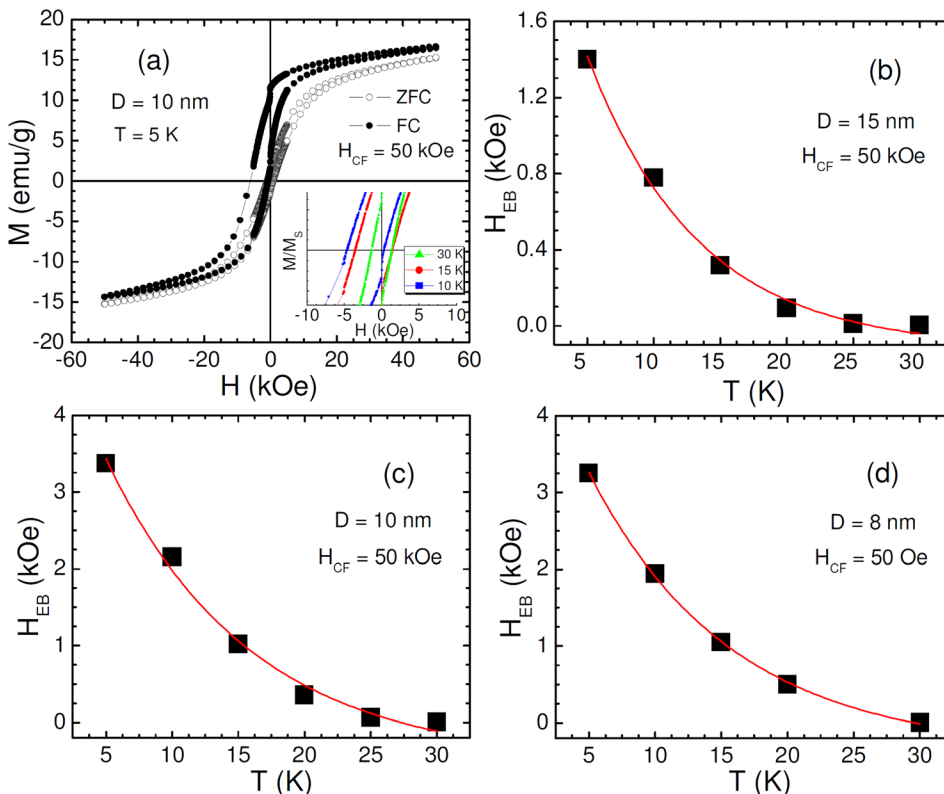


FIG. 3. (a) ZFC and FC M-H loops taken at 5 K for sample A-10; its inset shows the FC M-H curves at different temperatures. Temperature dependence of exchange bias field H_{EB} for (b) 15 nm, (c) 10 nm, and (d) 8 nm Fe/ γ -Fe₂O₃ nanoparticles in a cooling field of 50 kOe.

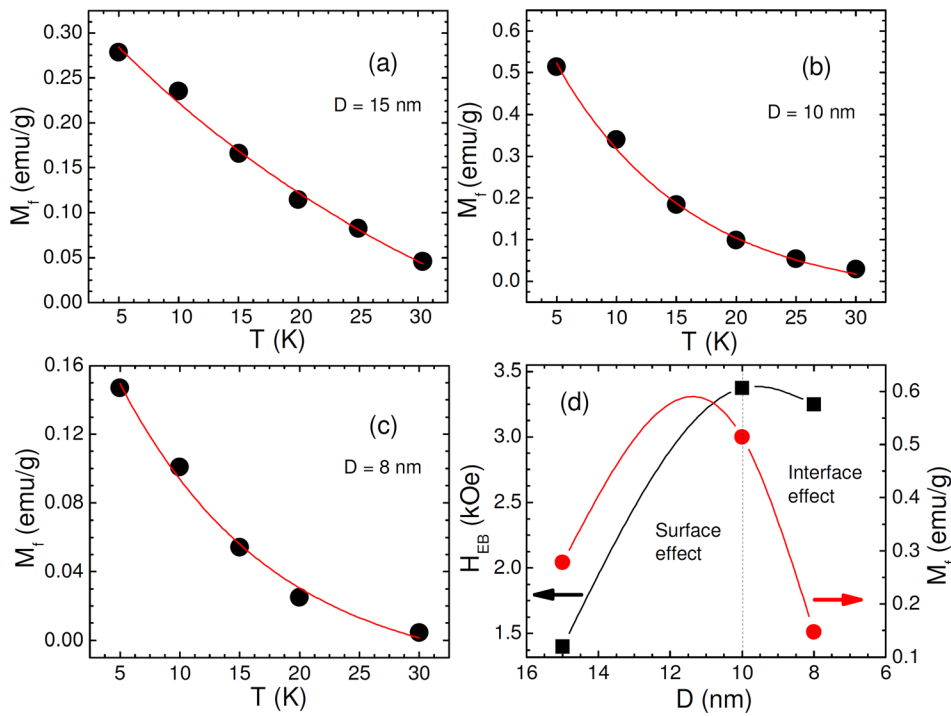


FIG. 4. Temperature dependence of the net moment of frozen spins (M_f) for (a) 15 nm, (b) 10 nm, and (c) 8 nm Fe/ γ -Fe₂O₃ nanoparticles. H_{EB} and M_f are plotted as a function of particle size (d).

$$M_f = \frac{1}{2}(M(H^+) - M(H^-)). \quad (2)$$

The M_f is proportional to the number of frozen spins, $S_F \propto M_f$.²¹ Since the shell thickness (t_{FIM}) remains constant in our particles, H_{EB} is directly related to the moment of irreversible spins and inversely related to the reversible spins ($M_R = M_{FM}$). Also, $M_R \sim M(H^+)$ and H_{EB} depends linearly on the ratio of number of frozen spins (M_f) to reversible spins

$$H_{EB} \propto \frac{M_f}{M(H^+)}. \quad (3)$$

Having applied Eq. (2) to calculate M_f from the M-H data for different temperatures below T_B , the temperature dependence of EB field (Figs. 3(b)–3(d)) can now be interpreted by considering the variation in the number and moment of interfacial frozen spins for a given particle size. Figures 4(a)–4(c) show the temperature dependence of M_f for all the samples. As one can see clearly in this figure, M_f approaches zero at a temperature above which EB vanishes, pointing to the direct impact of M_f upon H_{EB} . It is worth noting that with the decrease in particle size from 15 nm to 8 nm, M_f first increases, reaches a maximum for 10 nm particles, and then decreases for smaller particles (see Fig. 4(d)). This gives a simple explanation for the temperature dependence of H_{EB} (Figs. 3(b)–3(d)) and for the relationship between the population of interfacial frozen spins and the strength of exchange coupling (Eq. (3)) between the core and shell. As one can also see in Fig. 4(d), while the H_{EB} of sample A-15 is smaller than that of sample A-8, an opposite trend is observed for M_f in these two samples. These results point to the fact that the effect of disordered surface spins is strongest in the smallest particles (sample A-8) and thus contributes dominantly to the EB. Recent studies have revealed that the interfacial magnetic coupling can be strengthened by the enhanced disordering of surface

spins.^{14,15,22} This may explain the largest value of M_f obtained for the 10 nm particles relative to other particle sizes. Further experimental and theoretical studies are needed to affirm this.

To reaffirm the importance of surface spin disorder, we have quantified the superparamagnetic (SPM) and paramagnetic (PM) contributions to the magnetization by fitting the room temperature M-H data to the Langevin function with an added linear term as⁵

$$M(H) = M_s^{SPM} \left[\coth\left(\frac{\mu H}{KT}\right) - \left(\frac{\mu H}{KT}\right)^{-1} \right] + C^{PM} H, \quad (4)$$

where M_s^{SPM} is the saturation magnetization of the SPM part and μ is the average magnetic moment of SPM particles. C^{PM} is the susceptibility of the paramagnetic contribution that is linear with the magnetic field H . The experimental and fitted M-H curves are shown in Figs. 5(a)–5(c) for all the samples. It can be seen that for the largest particles (sample A-15), the SPM susceptibility contributes 85% to the total observed experimental magnetic moment, while the rest of it is the PM susceptibility (15%). With further decrease in the particle size, the contribution from the SPM susceptibility decreases significantly to 55% for 10 nm particles (sample A-10) and 15% for 8 nm particles (sample A-8), whereas the contribution from the PM susceptibility increases strongly to 45% and 85%, respectively. It has been pointed out that the very high linear contribution to the magnetization is from the uncompensated spins at the particle surface and crystallite interfaces, which are strongly pinned along a local axis due to surface anisotropy.^{5,13} Therefore, the increasing contribution to the magnetization from the PM susceptibility with the decrease in particle size is fully consistent with the perspective that surface spins are more disordered and their impacts are stronger in smaller particles. For the case of sample A-8 (the smallest particle), the largest contribution to the magnetization from

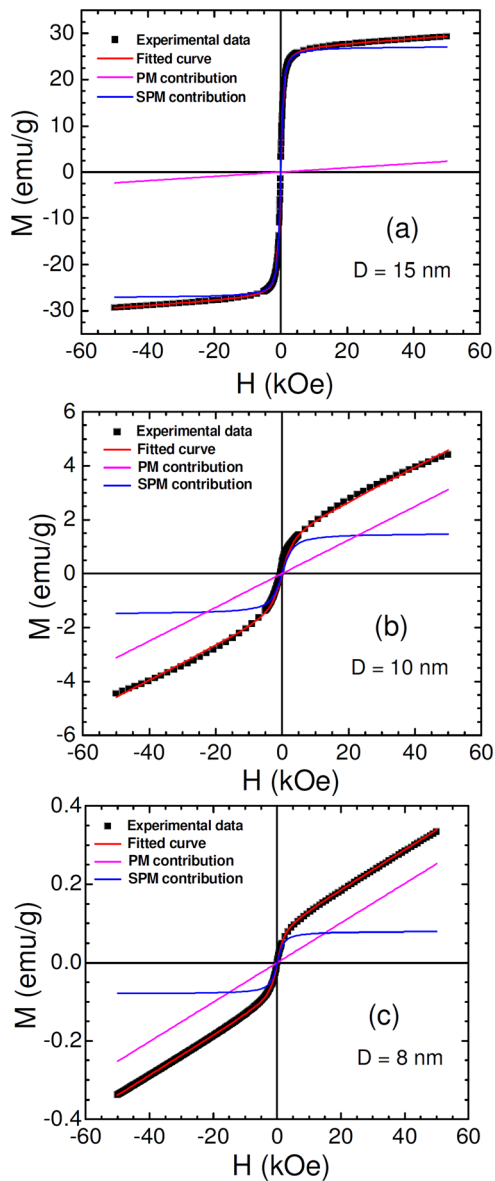


FIG. 5. The M-H curves at 300 K are fitted (red) to Eq. (4); the blue and magenta (dashed) curves represent the simulated SPM and PM contributions extracted from the experimental data using the fitting parameters for (a) 15 nm, (b) 10 nm, and (c) 8 nm $\text{Fe}/\gamma\text{-Fe}_2\text{O}_3$ nanoparticles.

the PM susceptibility implies that the strongest disordering effect of surface spins occurs in this sample.

In summary, we have demonstrated the existence of a critical particle size (~ 10 nm for the case of the $\text{Fe}/\gamma\text{-Fe}_2\text{O}_3$ nanoparticles studied in this work), above which the interface spin effect contributes primarily to the EB, but below which the surface spin effect dominates. Our study yields

physical insight into the underlying origin of the EB effect in core-shell nanoparticle systems and provides an effective way for optimizing EB in such magnetic nanostructures for spintronics applications.

The research was supported by the Center for Integrated Functional Materials through Grant No. USAMRMC W81XWH-10-2-0101 (synthesis and structural characterization of samples) and by the DOE through Grant No. DE-FG02-07ER46438 (magnetic studies). M.H.P. acknowledges support from the Florida Cluster for Advanced Smart Sensor Technologies. The authors would like to thank Paula Lampen for editing the manuscript and helpful discussions.

- ¹J. Nogues and I. K. Schuller, *J. Magn. Magn. Mater.* **192**, 203 (1999).
- ²O. Iglesias, A. Labarta, and X. Batlle, *J. Nanosci. Nanotechnol.* **8**, 2761 (2008).
- ³S. Laureti, S. Y. Suck, H. Haas, E. Prestat, O. Bourgeois, and D. Givord, *Phys. Rev. Lett.* **108**, 077205 (2012).
- ⁴X. L. Sun, N. F. Huls, A. Sigdel, and S. S. Sun, *Nano Lett.* **12**, 246 (2012).
- ⁵H. Khurshid, W. F. Li, M. H. Phan, P. Mukherjee, G. C. Hadjipanayis, and H. Srikanth, *Appl. Phys. Lett.* **101**(2), 022403 (2012).
- ⁶K. Simeonidis, C. Martinez-Boubeta, O. Iglesias, A. Cabot, M. Angelakeris, S. Mourdikoudis, I. Tsiaoussis, A. Delimitis, C. Dendrinos-Samara, and O. Kalogirou, *Phys. Rev. B* **84**, 144430 (2011).
- ⁷B. Martinez, X. Obradors, L. Balcells, A. Rouanet, and C. Monty, *Phys. Rev. Lett.* **80**, 181 (1998).
- ⁸T. N. Shendruk, R. D. Desautels, B. W. Southern, and J. van Lierop, *Nanotechnology* **18**, 455704 (2007).
- ⁹R. D. Desautels, E. Skoropata, Y.-Y. Chen, H. Ouyang, J. W. Freeland, and J. van Lierop, *Appl. Phys. Lett.* **99**, 262501 (2011).
- ¹⁰R. D. Desautels, E. Skoropata, Y.-Y. Chen, H. Ouyang, J. W. Freeland, and J. van Lierop, *J. Phys.: Condens. Matter* **24**, 146001 (2012).
- ¹¹R. K. Zheng, G. H. Wen, K. K. Fung, and X. X. Zhang, *Phys. Rev. B* **69**, 214431 (2004).
- ¹²S. Chandra, H. Khurshid, W. F. Li, G. C. Hadjipanayis, M. H. Phan, and H. Srikanth, *Phys. Rev. B* **86**, 014426 (2012).
- ¹³I. Panagiotopoulos, G. Basina, V. Alexandrakis, E. Devlin, G. Hadjipanayis, L. Colak, D. Niarchos, and V. Tzitzios, *J. Phys. Chem. C* **113**, 14609 (2009).
- ¹⁴Y. Hwang, S. Angappane, J. Park, K. An, T. Hyeon, and J. G. Park, *Curr. Appl. Phys.* **12**, 808 (2012).
- ¹⁵Q. K. Ong, X. M. Lin, and A. Wei, *J. Phys. Chem. C* **115**, 2665 (2011).
- ¹⁶Q. K. Ong, A. Wei, and X. M. Lin, *Phys. Rev. B* **80**, 134418 (2009).
- ¹⁷R. F. L. Evans, D. Bate, R. W. Chantrell, R. Yanes, and O. Chubykalo-Fesenko, *Phys. Rev. B* **84**, 092404 (2011).
- ¹⁸H. Khurshid, W. F. Li, V. Tzitzios, and G. C. Hadjipanayis, *Nanotechnology* **22**, 265605 (2011).
- ¹⁹H. Khurshid, V. Tzitzios, W. F. Li, C. G. Hadjipanayis, and G. C. Hadjipanayis, *J. Appl. Phys.* **107**, 09A333 (2010).
- ²⁰W. H. Meiklejohn and C. P. Bean, *Phys. Rev.* **105**, 904 (1957).
- ²¹H. Khurshid, S. Chandra, W. Li, G. C. Hadjipanayis, P. Mukherjee, M. H. Phan, and H. Srikanth, *J. Appl. Phys.* **113**, 17B508 (2013).
- ²²H. Khurshid, S. Chandra, W. Li, G. C. Hadjipanayis, P. Mukherjee, M. H. Phan, and H. Srikanth, *Nanoscale* **5**, 7942 (2013).
- ²³A. Cabot, A. Paul Alivisatos, V. F. Puentes, L. Balcells, O. Iglesias, and A. Labarta, *Phys. Rev. B* **79**, 094419 (2009).